Performance Evaluation of a New CZT Detector for Nuclear Medicine: SOLSTICE

Jerome J Griesmer, *Member, IEEE*, Barry Kline, *Member, IEEE*, Joe Grosholz, Kevin Parnham, Daniel Gagnon, *Member, IEEE*

Abstract *- **Solstice is a new concept of gamma camera designed to use the better energy resolution typically available in solid-state detectors. To that purpose, an array of 88 Cadmium Zinc Telluride (CdZnTe or CZT) crystals was characterized for gamma ray detection performance. The bias voltage was applied to the single electrode cathode side of the crystal (radiation side). The anode side of the individual crystals was further subdivided into 32 anodes connected to a charge sensitive preamplifier/shaper circuit for each pixel that provided a virtual ground potential for the anodes. Overall, the vast majority of pixels (85%) of pixels had an energy resolution (FWHM) better than 5% at 140 keV and an outstanding 3.6% FWHM at 140 keV was measured for the overall composite energy resolution over this large population of pixels. Results from the crystal characterization along with overall system performance are discussed. The imaging performance of the detector is covered in a separated paper at this conference [1].***

I. Introduction

The need for better energy resolution in gamma camera has been expressed since soon after its invention by Anger in 1958. While constant progress has been made in this respect, the future does not hold much hope of a significant improvement if the basic detection scheme is not changed.

Solid-state detection devices, in particular the ones using CdZnTe (CZT), have been investigated for years without realizing any practical impact for imaging but seem now to offer a real possibility for practical and commercially affordable implementation. This paper describes the performance of a new CZT detector designed for nuclear medicine. It addresses strictly the electrical and physical performances; the imaging component being independently covered in a paper presented at this conference [1].

Several aspects of the development of a CZT detector will be covered. While a substantial amount of papers and information is available in the literature on the basic physics and signal processing of CZT, this paper clearly aims to address the significant engineering challenges that harnessing the power of semi-conductor detection represents. First, the major system components will be described. Second, a more detailed characterization of the CZT crystals/pixels within the system will be made and attempts to estimate global performance of the array in imaging conditions will be made.

- J.J. Griesmer, B. Kline and, D.Gagnon are with Philips Medical Systems, Nuclear Medicine, 595 Miner Road, Cleveland, OH, 44143.

- J.Grosholz and K. Parnham are with eV-Products, 373 Saxonburg Blvd, Saxonburg, PA, 16056

- For correspondence, daniel.gagnon@ieee.org

II. System Components

The Solstice system (for **SOL**id **ST**ate **I**mager with **C**ompact **E**lectronics) can be decomposed in three major components. First, the CZT configuration itself in terms of dimension and pixelization, second, the analog processing and pre-amplification of the signal, and thirdly, the overall data flow and various additional corrections and compensation of the acquisition system.

A. CZT Geometry

The current study on CZT performance was made during the construction of the Solstice prototype. A total of 88 CZT crystals have been included in these tests and are believed to be representative of what the technology can deliver. The bias voltage was applied to the single electrode cathode side of the crystal. The anode side of the individual crystals was further subdivided into 32 anodes (pixels, see Figure 1) connected to an ASIC charge sensitive preamplifier-shaper circuit for each pixel that provided a virtual ground potential for the anodes. The improvement in energy resolution of CZT arrays by using sub-pixelation has been previously reported by others [3].

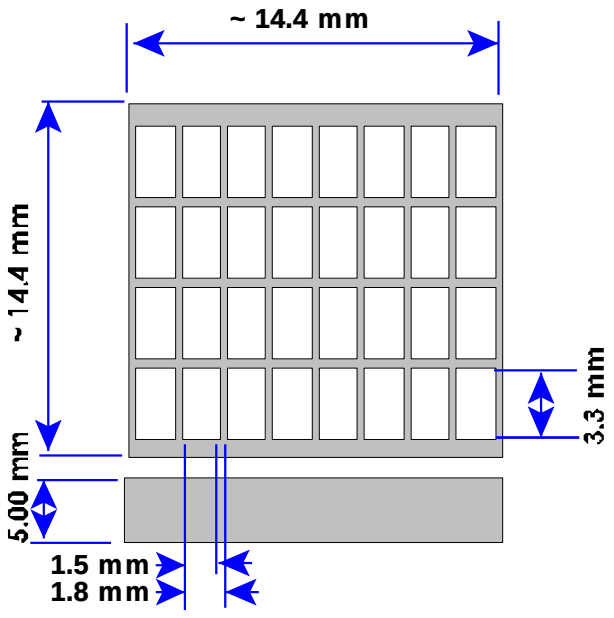

Figure 1. Pixel configuration and typical dimensions of the individual CZT crystals.

B. Pre-Amp Noise and System Noise

The analog noise of the ASIC preamplifier circuit [2] is a critical design parameter. The specification for the device used was 80 + 15/pF electrons RMS. With a 2.8 pF pixel added, the resulting total would be 122 electrons RMS. For a gain of 0.2V/fC, and using 2.4 = FWHM*Vpk/VRMS and 2.06 fC/60 keV, we can predict a FWHM of 1.2% for a 116 kV equivalent pulse (equivalent value in keV of the test pulses that can be injected in the system for test and QC purposes). Actual measurements produced 1.7% FWHM for the ASIC, PCB and connector without crystal and 2.3% FWHM (235 electrons RMS) for the same test pulse with crystal. These are slightly higher than expected, but still under half of the 5% target system performance and introduces only an added 0.5% to the FWHM value (analog and quantum noise being added in quadrature).

We also determined that one HV bias level would be used for all crystals in the array. Thus the crystal material and processing must be capable of producing pixels that behave within a limited range of properties.

Another parameter that was evaluated was the threshold voltage used. We determined that the preamplifier ASICs offset voltage and noise were within a narrow enough range to allow a single comparator voltage to be used for all pixels. The required performance was to not trigger on the noise from the high gain, high offset pixels, while ensuring that the lowest gamma design energy would exceed the threshold for the lowest gain and lowest offset pixels.

C. Basic Data Flow and Digital Path

The Solstice camera is functionally segmented into subgroups of 64 pixels each. Each subgroup is treated as an independent section of the overall imaging detector. Within the subgroup, asynchronous analog pulses from the preamp/shaper ASICs compete for access to a single analog output port via a "winner-takes-all" arbitration circuit. Each successful pulse is multiplexed to a free-running analog-to-digital converter (ADC). The data stream from the ADC is analyzed by digital peak-detection circuitry, and the energy measurement, along with the address of the winning pixel, are stored in a local FIFO memory for subsequent readout to a global acquisition memory. The peak-detection circuit, having determined the event's energy content and location, then releases the arbitration logic to accept another event.

The data packets containing event energy and location from the 64-pixel subgroups are transferred via a global readout bus using a token-passing arbitration scheme. The architecture of the detector design packs four peak-detectors and one FIFO into a FPGA. The stored event data from each FIFO is placed on the readout bus as the token signal is received. A final FPGA packs the event data along with time stamps and other protocol for transmission to an image data acquisition computer.

The projected rate capabilities of the Solstice detector are determined by the dead times associated with the independent 64-pixel subgroups. The primary contributors to that dead time are the time-to-peak for the shaped analog pulse, ADC pipeline delay, and the time required for the peak-detection and FIFO storage circuitry to operate. In the present design, this combined dead time is 1.7 usec per event. As the system incorporates no pileup rejection at the 64-pixel level, each subgroup follows a non-paralyzable throughput rate limitation of 118 kcps at the 20% loss point. Because each of the subgroups operates independently, the throughput rate will scale linearly with the number of subgroups. The current design is scalable; the projected throughput rate for the 3072-pixel prototype detector, comprising 48 such subgroups, should approach 5.6Mcps at the 20% loss point.

In practice, the achievable rate is limited by the digital acquisition and framing hardware and software. The current prototype can run at 650 Kcps and will be increased to more than a 1 Mcps in the next revision. Figure 2 summarizes the basic functions and data flow.

The extent of the processing of the digital signal before actually performing imaging (framing) is to apply an offset and gain to the energy signal and the application of a conventional uniformity correction to compensate for all remaining non-idealities of the detection system.

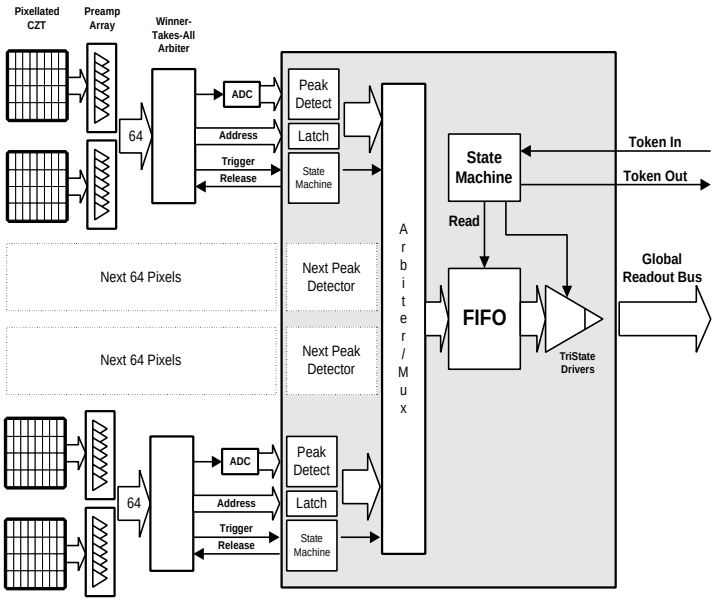

Figure 2. Basic functions and data flow/data reduction in the Solstice camera. With the current architecture and dead time characteristics, several millions counts per second can be achieved with the detector without any loss in performance.

III. CZT CHARACTERIZATION

The performance evaluation of an imaging system is a complex task. We will review in this section some of the more explicit in the following comments.

A. Temperature

Early analysis of the heat dissipation from the ASIC and support parts showed significant problems. With close to 24mW per channel for the ASIC (46 mW per channel including the support chips) and the anticipation of several

thousand channel required in a useful gamma camera (close to 3000 tested in this prototype), proper cooling of the array is essential. As is typical for semi-conductors, the leakage current has a high order positive relationship to temperature and excessive leakage current introduces additional analog noise that increases the energy resolution FWHM. An innovative daughter/mother board structure was devised to allow adequate cooling using only ambient air flow. The configuration allowed sufficient air flow across the ASIC limiting the temperature rise above inlet ambient to only 16 ºC on the ASIC package and only 6 to 8 ºC rise on the CZT crystals. This kept the leakage currents on the CZT crystals to a acceptable performance level.

B. Bias Voltage

After exposure to a uniform (line) source, spectrums of each individual pixel can be extracted and analyzed and additionally sub grouped as crystal averages and a global average can be calculated. The global average FWHM can also be measured directly by standard NEMA methods. The FWHM performance of the array to a variation of the cathode bias voltage was then studied.

1. Crystal Averages

Graphs of the Figure 3 summarizes the findings for the crystal averages. Each curve show the measured average energy resolution per crystal, ranked from best to worst at the reference voltage. The order of the crystals is then maintained for all the subsequent curves.

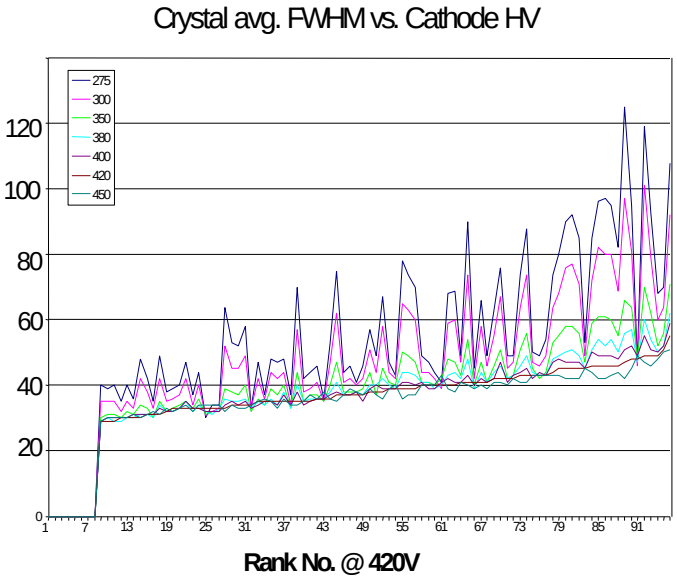

Figure 3. Energy resolution of individual crystal as a function of the applied voltage on the cathode. Ranking of crystals has been obtained at 420 V and maintained for all the other curves, Vertical axis in FWHM of energy resolution x 10. At 420 V the average of ALL crystals is below 6%

It is first interesting to note that while a general trend exists and seems to favor higher voltages, sensitivity to a variation in the high-voltage is high dependent on the crystal under consideration: Some crystals being essentially insensitive to the bias voltage, while others may double their energy resolution. A bias voltage of 420 V was finally implemented.

2. Individual Pixel Characteristics

Global performance of the individual pixel (as measured by the energy resolution) showed interesting behavior. A detailed analysis of individual energy spectra showed some unexpected results. Families of pixels were created according the shape of the energy spectrum and to the response of the pixel to a variation of voltage. First, the vast majority of pixels was well behaved and had a classical energy spectrum. Energy resolutions as low as 2.7% were measured by the system. Figure 4 shows a typical pixel with an energy resolution of 3.6% FWHM for ^{57}Co (same as the composite average for the whole array).

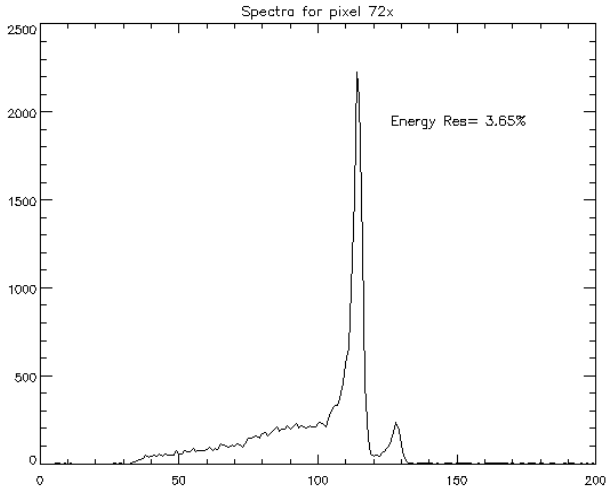

Figure 4. Energy spectrum for pixel 72x measured at 3.65% FWHM for ^{57}Co

In the following series of pairs of spectrum, we are illustrating the different pixel behavior. The lower voltage, 275 V, is on the left, the higher voltage, 420 V, is on the right. Comments are below each pair. Since the unusual response pixels are adjacent to "typical" response pixels, this may be attributed to the effects of local crystal structure variations. Similar effects have been reported by others [4, 5]. The challenge for the CZT supplier is to provide crystals with fewer defect areas within each crystal. Substantial improvements have been achieved since the first devices tested. It is also a characteristic of the Solstice imaging device that defective pixels do not produce any effect on the resultant image quality. The result of a dead pixel is only a small reduction in sensitivity. This has significant impact on the cost implications for crystal production.

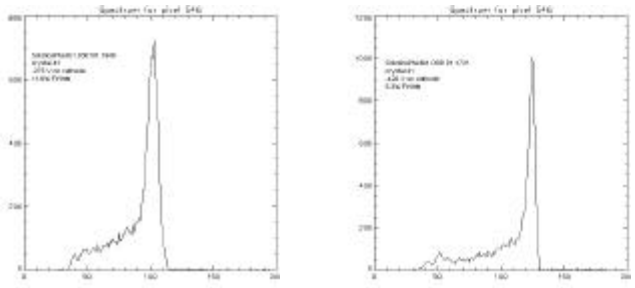

Pixel #546, Typical. ~89% of all pixels. Overall shift and broadening of the peak at low bias

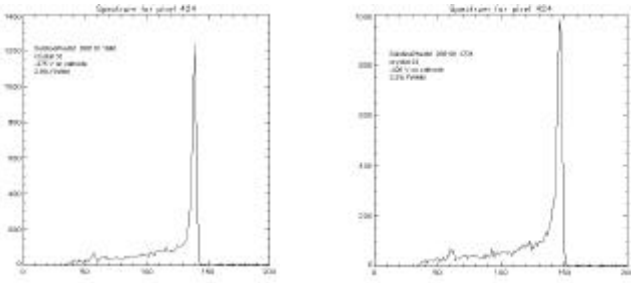

Pixel #424, Improvement at low bias. ~5% of all pixels. Overall shift and narrowing of the peak at low bias

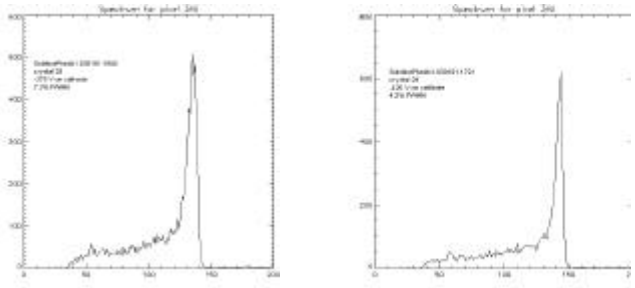

Pixel #3f6. Split Peak at low bias. ~5% of all pixels. Overall shift and broadening of the peak at low bias

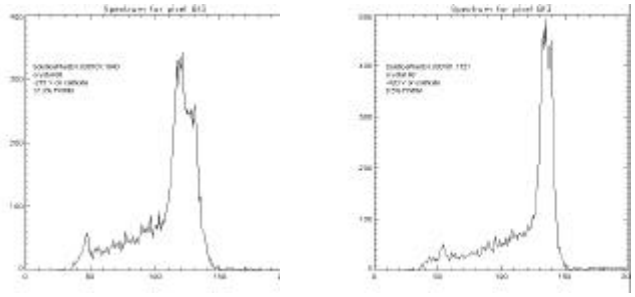

Pixel #8f3. Split Peak at low and high bias. 0.5% of all pixels. Overall shift and broadening of the peak at low bias

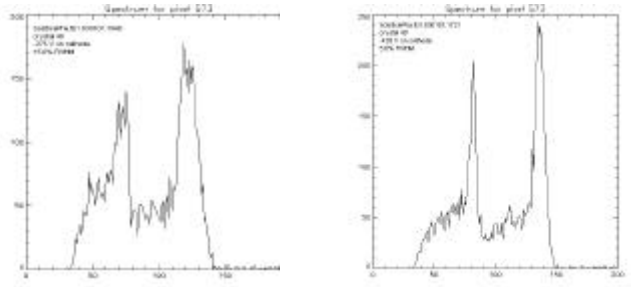

Pixel #573. Double peak. 0.04% of all pixels. Overall shift and broadening of the peak at low bias

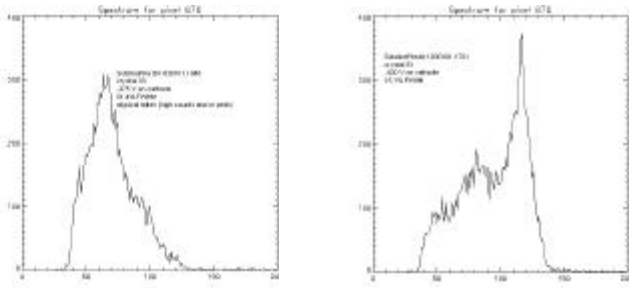

Pixel #670. Unusable. 0.1% of all pixels. Overall shift and broadening of the peak at low bias

Overall, pixels with split spectrum, double peaks or otherwise non-standard shape represented less than 1% of all the pixels.

Additional tests performed by swapping crystal positions in the array confirm that the dominant response is the CZT crystal itself and the analog and digital noise contributions are minimal.

IV. DISCUSSION

We have demonstrated in part II of this paper that the overall system surrounding the CZT, more specifically the ASIC preamp, the data flow and data arbitration, the conversion to digital and the application of the various corrections, is well under control and that we indeed measuring the performance of the CZT itself. This point is critically important as, contrary to other gamma ray detection schemes, detection material AND processing electronics are very intimately related. All the steps leading to forming a spectrum such as the one presented in Figure 4 for several thousand pixels, at close to half a million counts per second, AND maintaining 3.6% overall energy resolution is a strong indicator of the quality of the system.

It also means that our observations on the different behavior of crystals and/or pixel are valid and do constitute a good basis for a more thorough analysis. Questions like: is a global threshold for the triggering system possible and adequate, what is the performance penalty in setting a global voltage for all the crystals, what is influencing the baseline for each individual channel, effect of temperature on the performance of the CZT and on the ASIC? All these questions will have a direct influence on the complexity (and cost) of any larger scale utilization of CZT in a gamma camera.

In addition, having produced some of the results very early in the development of the prototype, refinements in the process of building and testing the crystals have been identified and will be part of the next iteration of device. In particular the process improvement identified in the construction of the crystal modules, that need to be easily removable for servicing, should bring better quality. Similarly, we have experienced reliability issues with the construction of the ASICs that have since then been identified, corrected and fully tested.

V. Conclusion

It is believed that the results presented in this paper are among the best ever published for a large number of CZT crystals/pixels at room temperature. This is obviously a very important element in making the decision to build gamma camera based on CZT, but more is required. We have explored several aspects of the required "surrounding" technology and the results obtained so far indicate that the current combination of CZT-ASIC-Data Reduction is very flexible, scalable and would lend itself efficiently to a commercial implementation.

VI. Acknowledgements

The authors would like to thank the members of the engineering team, Austin Bowen, Bob Davis, Eric Dillen, Harry Smith and Steve Vydrin from eV-Products, and Pat Bender, Kevin Mantey , Kevin McMahon, Jason Radachy and Bob Zahn at Philips Medical Systems.

VI. References

[1] GL.Zeng, D. Gagnon, CG. Matthews, JA. Kolthammer, JD. Radachy *"Image Reconstruction Algorithm for Rotating Slat Collimator"* IEEE MIC 2001, San Diego, Nov. 2001.

[2] DeGeronimo G, O'Connor, Grosholz J. *"A Generation of CMOS Readout ASICx for CZT Detectors"*, Proc of IEEE Nuclear Science Symposium, Seatle, WA, Nov. 1999.

[3] Eskin JD. Et al. "*The Effect of Pixel Geometry on Spatial and Spectral Resolution of CdZnTe Imaging Array"*, Proc. of IEEE Nuclear Science Symposium, pp.544-548, San Francisco, CA, Oct. 1995

[4] Amman M, et al. "*CdZnTe Material Uniformity and Coplanar-Grid Gamma-Ray Detector Performance"*, IEEE Trans Nucl. Sci.,vol 47, no 3, June 2000.

[5] Brunnett BA, "The Performance Effect of Crystal Boundaries in Cadmium Zinc Telluride Radiation Spectrometers". IEEE Trans Nucl. Sci.,vol 47, no 4, Aug. 2000